The metallicity properties of zCOSMOS galaxies at 0.2<z<0.8

G. Cresci[1]⋆, F. Mannucci[1], V. Sommariva[1], R. Maiolino[2], A. Marconi[3], M. Brusa[4]

[1] *INAF - Osservatorio Astrofisico di Arcetri, Largo E. Fermi 5, 50125 Firenze, Italy*
[2] *INAF - Osservatorio Astronomico di Roma, via di Frascati 33, 00040 Monteporzio Catone, Italy*
[3] *Università di Firenze - Dipartimento di Fisica e Astronomia, Largo E. Fermi 2, 50125 Firenze, Italy*
[4] *Max Planck Institut für extraterrestrische Physik, Postfach 1312, 85741 Garching, Germany*

ABSTRACT

We study the metallicity properties of galaxies in the zCOSMOS sample between $0.2 < z < 0.8$. At $z < 0.46$, where Hα and [NII] are detected, we find the same dependence of metallicity on stellar mass and Star Formation Rate (SFR), the Fundamental Metallicity Relation, found by Mannucci et al. (2010) in SDSS galaxies on a similar redshift range. We extend this relation to higher redshift, $0.49 < z < 0.8$ where the R_{23} metallicity index can be measured in our data, finding no evidence for evolution, and a metallicity scatter around the relation of about 0.16 dex. This result confirms, with a much higher level of significance with respect to previous works, the absence of evolution of the FMR during the last half of cosmic history.

Key words: Galaxies: abundances; Galaxies: formation; Galaxies: high-redshift;

1 INTRODUCTION

The Fundamental Metallicity Relation (FMR) is a tight relation between stellar mass, SFR, and metallicity, discovered by Mannucci et al. (2010, hereafter M10) using local SDSS galaxies. The gas-phase metallicity of $\sim$140.000 galaxies with redshift between 0.07 and 0.3 is found to depend not only on stellar mass, in the well-known mass-metallicity relation (Tremonti et al. 2004), but also on SFR, with more active galaxies showing lower metallicities. After considering this relation, the residual metallicity scatter is limited to $\sim$0.05 dex, which is compatible with the effect of the uncertainties on mass, SFR, and metallicity.

The role of specific SFR (SSFR=SFR/Mass)) in relation with metallicity was first suggested by Ellison et al. (2008), who presented a mild (~ 0.1 dex) dependence of metallicity on SSFR when binning galaxies according to their stellar mass. After M10, Lara-López et al. (2010) discussed a plane in the same 3D space, and proposed to use it to derive the stellar mass of galaxies once their SFR and metallicity is known. The exact shape of the relation, especially at the high mass end, depends on the choice of the metallicity calibrations, on the assumptions about dust extinction and SFR, and on the extent of the aperture corrections allowed, as reported in Yates et al. (2011).

Although the presence of the FMR is well established

at low z, regardless of the metallicity calibration used, only a limited amount of distant galaxies have been used for the study of the FMR at high redshifts. The data available show that no evolution is present up to z=2.5, see Fig. 4 of M10), i.e., galaxies of any mass and SFR follow the same FMR defined by local galaxies. The observed evolution of the mass-metallicity relation (e.g. Maiolino et al. (2008), Mannucci et al. (2009)) is therefore due to a prospective effect, as high redshift galaxies usually have higher SFR and, as a consequence, lower metallicities. Some evolution is observed at even higher redshifts, z>3, as discussed in M10 and Troncoso et al. (in preparation).

This results has been later confirmed by several groups. For example, Richard et al. (2011) studied a sample of lensed galaxies at 1.4<z<5, which have SFR smaller than the other samples of un-lensed galaxies at these redshifts (Erb et al 2006, Maiolino et al. 2008, Mannucci et al. 2009). These galaxies show higher metallicity with respect to the mass-metallicity relation, exactly as expected by the FMR. Similarly, Nakajima et al. (2011) presented the metallicities of stacked Lyα emitter at $z \sim 2.2$, which have smaller SFR than other galaxies at similar redshift, but also higher metallicities according to the FMR. On the other hand, various highly star forming galaxies at high redshift are presented in the literature as very metal poor for their stellar mass. However, they result to be consistent with the FMR once their high SFR is considered (e.g. Erb et al. 2010, Kassin et al. 2011). Finally, the use of the FMR allowed Mannucci et al. (2011) to show that, when

⋆ E-mail:gcresci@arcetri.astro.it

considering their high SFRs, the host galaxies of long-GRBs have the same metallicity distribution of field galaxies.

The high redshift galaxy samples used by M10 show a much larger spread in metallicity ($\sim$0.25 dex) around the FMR than local SDSS galaxies ($\sim$0.05 dex). The spread is comparable with the much larger uncertainties in SFR and metallicity, due to the generally lower signal-to-noise (S/N) ratio of the detected emission lines. This large spread could hide systematic trends, therefore it is important to test this results using larger samples of galaxies. In this paper we use data from the zCOSMOS survey to study the evolution of the FMR up to $z \sim 0.8$ with higher precision. This is fundamental to understand if the same long lasting equilibrium between star formation, infall of pristine gas and outflow of enriched material that seems to be responsible for the FMR in local galaxies (see e.g. Davé et al. 2011, Torrey et al. 2011) is also driving galaxy evolution at higher redshift, where infalls (Erb 2008, Mannucci et al. 2009, Cresci et al. 2010) and outflows (e.g. Steidel et al. 2010) are expected to be even more relevant.

The paper is organized as follows. In Sect. 2 we briefly introduce the sample used, in Sect. 3 we present the method used to derive the stellar masses and in Sect. 4 we described how the line fluxes and the final sample selection were obtained. The measures of SFRs and extinctions are discussed in Sect. 5, while those of metallicities in Sect. 6. Our results are discussed in Sect. 8, while our conclusions follow in Sect. 9.

2   THE ZCOSMOS SAMPLE

zCOSMOS (Lilly et al. 2007) is a redshift survey in the COSMOS field using the VIMOS multi-object spectrograph on ESO/VLT. It consists of two parts: the first, zCOSMOS-bright, is a redshift survey of $\sim$ 20000 I-band selected galaxies at redshifts $z < 1.2$, covering the approximately 1.7 deg^2 of the COSMOS field; the second part, zCOSMOS-deep, is observing $\sim$ 10000 galaxies selected through well-defined color selection criteria and at B¡25 to be in the redshift range $1.5 < z < 3.0$. These observations are restricted to the central 1 deg^2 of the COSMOS field. Here we have used the spectra of the data release 2 of the zCOSMOS-bright survey, the so-called "10k-bright", available on the project web site since 1 Oct 2008[1]. These consist of $\sim$ 10000 spectra, obtained with 1$''$ wide slits and the MR grism (R$\sim$600 with a wavelength range of approximately 5550 to 9650 Å, sampled at roughly 2.5 Å/pixel). The details about the object selection, observations and data reduction can be found in Lilly et al. (2009).

In order to measure gas phase metallicity for our galaxies using strong optical emission lines, we need either [NII]λ6584 and Hα, or [OII]λ3727, [OIII]λ5007 and Hβ visible in the wavelength range of the VIMOS spectrum. We therefore divided the obtained sample in two subsample at different redshifts: 2825 galaxies at $z < 0.47$ have accessible

Hα emission and 3691 galaxies at $z > 0.49$ are in the right redshift range to observe [OII] emission. [OIII]λ5007and Hβ are observable for all these galaxies.

3   MASS AND CONTINUUM SPECTRA FROM SED FITTING

To estimate the stellar masses we used 12 photometric bands: CFHT u^* and K_s, Subaru B_j, V_j, g^+, r^+, i^+ and z^+, UKIRT J (Capak et al. 2007, Ilbert et al. 2009), and Spitzer IRAC at 3.6 μm, 4.5 μm and 5.8 μm (Frayer et al. 2009).

The photometry for all the optical and near-IR bands were measured over an aperture of 3$''$ diameter, to minimize the effect of Point Spread Function variation from band to band. The derived fluxes are then corrected to total using the so called "auto-offsets", derived from the i-band image comparing the 3$''$ magnitude with the SExtractor total one (see Capak et al. 2007). The IRAC fluxes were measured in a circular aperture of radius 1.9$''$, converted to total fluxes using the correction factors derived by Surace et al. (2004). We also used GALEX FUV and NUV photometry from Zamojski et al. (2007), when available. A few galaxies show problematic values of the magnitude (Bolzonella et al. private communication), therefore GALEX photometry was only used when the reduced χ^2 of SED fitting is below 2, for a total of 64 galaxies.

The stellar masses were obtained with a Spectral Energy Distribution (SED) fitting analysis, using the HyperZmass code (Pozzetti et al. 2007, Pozzetti et al. 2009), a modified version of the HiperZ code (Bolzonella et al. 2000): the observed photometric SEDs are compared to those obtained from a set of reference synthetic spectra from stellar population models, and the best fitting SED is obtained using a χ^2 minimization. The best fitting spectrum and its normalization provide estimates of the star formation rate, extinction, stellar population age and galaxy stellar mass (as the integral of the SFR over the obtained age, correcting for mass losses during stellar evolution, see Pozzetti et al. 2007). In addition, the code makes available in output the best fitting synthetic stellar continuum for each galaxy, that has been used to correct for the Balmer absorptions (see Section 4).

The reference spectral library was built with the Bruzual & Charlot (2003) code for spectral synthesis models, using the low resolution version with the Padova 1994 tracks. The models were produced assuming a Chabrier Initial Mass Function (IMF) (Chabrier et al. 2003) with an upper mass limit of $100 M_{\odot}$, the Calzetti (2000) extinction law with A$_V$ varying between $0 - 4$ mag, and fixing the redshift to the spectroscopic value. We used smooth exponentially decreasing Star Formation Histories, with time scale τ in the range $0.1 - \infty$ and age t between $0.1 - 20$ Gyr. An example of SED fitting for one of the galaxies of our sample is shown in Fig. 1.

The stellar masses computed by Kauffmann et al. (2003a) for the SDSS sample used by M10 to derive the FMR in the local universe were instead computed using random secondary bursts in addition to the single one used here.
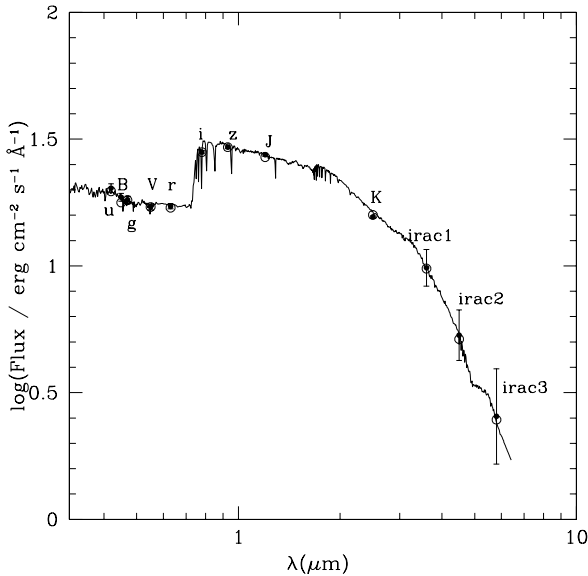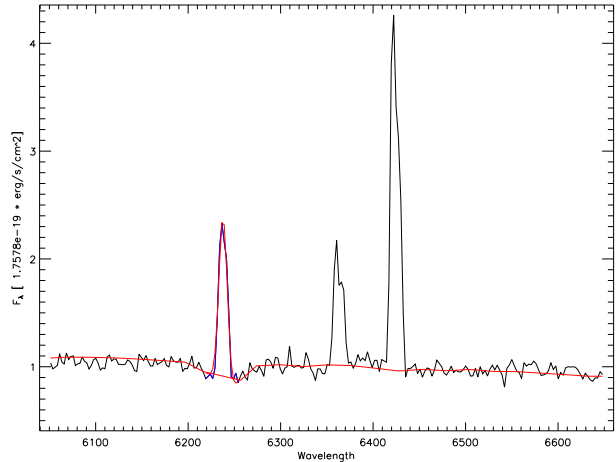
Figure 1. Example of SED fitting for one of the galaxies in the sample, ZC803435. The observed photometric data are shown as black solid points, while the expectations for each band based on the synthetic spectrum are shown as empty points.

Figure 2. Example of the measurement of line fluxes by using the continuum obtained with SED fitting for one of the galaxies in the sample, ZC817676. The observed spectra is shown in black, while the continuum model and the best fitting Gaussian for the Hβ line are shown in red. The [OIII] doublet is also visible in the spectral region shown.

Previous studies (e.g. Fontana et al. 2004, Pozzetti et al. 2007) have shown that random secondary bursts may produce systematically larger masses up to about 0.2 dex. We therefore run several tests adding random secondary burst to our synthetic spectra to check if this systematic difference in the stellar mass due to the use of a single exponential star formation history in our data is present and comparable to previous studies. In agreement to what is found in the literature, we found that the stellar mass obtained with random secondary burst are $\sim 0.15 - 0.2$ dex larger than the ones obtained with a single burst. We therefore added 0.2 dex to the stellar masses obtained with a single burst for consistency with the SDSS stellar masses. The stellar masses derived were also compared with the results obtained using the Maraston et al. (2005) spectral library, which include a more detailed treatment of the thermally pulsing asymptotic giant branch stars. These stars contribute significantly to the total luminosity in the $\sim 0.2 - 2$ Gyr stellar population age. We found that the stellar masses obtained using the Maraston et al. (2005) library are lower on average by a factor of ~ 0.1, as already mentioned in Bolzonella et al. (2010). To allow an easy comparison with the previous study in M10 for SDSS galaxies, we use in the following the results obtained with the Bruzual & Charlot (2003) library.

4 LINE FLUXES

The extracted 1-D spectra provided by the zCOSMOS release were used to measure emission line fluxes. For each spectrum we fitted several emission lines, [OII]λ3727, [NeIII]λ3869, Hγ, Hβ, [OIII]λ5007, [OIII]λ4959, [NII]λ6548, Hα, [NII]λ6584, [SII]λ6716, [SII]λ6730, when available in

the accessible spectral range (see Section 2). The fit was performed using a custom IDL code, which automatically fits with a χ^2 minimization a suitable stellar continuum and a Gaussian to each emission line.

To measure reliable fluxes, it is important to properly account for the stellar Balmer absorption, which in some galaxies can reach equivalent widths of $\sim$ 5Å. The best fitting synthetic stellar continuum derived from the SED fitting analysis of each galaxy (see Section 3) is used to reproduce the absorption line profile and the continuum shape. The synthetic stellar continuum is providing a very good representation of the observed continuum in all the inspected spectra, providing a good estimate of the absorption underlying the Balmer emission lines: an example is shown in Fig. 2.

The continuum is fitted in a region of ± 300 Å around the expected position of each emission line. During the minimization, pixels in the data that consistently deviated more than 3σ from the average were rejected, and were not used in the analysis. The uncertainties on the measured centroid position, velocity dispersion and flux are evaluated through Monte Carlo realizations, perturbing the input data assuming Gaussian uncertainties.

5 STAR FORMATION RATE AND EXTINCTION

SFR can be derived from the Hα and Hβ lines, which provide a direct probe of the young massive stellar population. Similar to what has been done in M10 and many other authors, we have used the classical conversion factor by Kennicutt (1998), scaling down the results by a factor of 1.7 (Pozzetti et al. 2007) to convert them to the Chabrier (2003) IMF. The conversion factor is based on the Hα or Hβ flux corrected for dust extinction, and therefore requires a good knowledge of the amount of extinction A_V suffered

by the emission lines.

For galaxies at $z < 0.47$, where both Hα and Hβ are visible, the extinction can be derived directly from the Balmer decrement Hα/Hβ, assuming a Calzetti (2000) extinction law, and the SFR from the Hα extinction corrected flux. At $z > 0.49$, where Hα is not visible anymore in our data, we used the Balmer decrement of the fainter Hγ/Hβ for all the galaxies where S/N(Hγ)$\geqslant$ 5, while the extinction $A_{V,SED}$ derived for the continuum by the SED fitting (see Section 3) for the other galaxies.

Calzetti et al. (2000) found evidence that the extinction derived from emission lines $A_{V,neb}$ in actively star forming galaxies is not equal but proportional to that measured from the continuum, with $A_{V,neb} = A_{V,SED}/0.44$ (see also e.g. Förster Schreiber et al. 2009). We have compared $A_{V,neb}$ and $A_{V,SED}$ for all the galaxies where a Balmer decrement extinction measurement is available (either Hα/Hβ or Hγ/Hβ), finding that the extra attenuation of the emission lines is confirmed by our data: our best fitting relation is $A_{V,SED} = (0.42 \pm 0.01) \cdot A_{V,neb}$. Given the small differences, we adopt the relation $A_{V,neb} = A_{V,SED}/0.44$ of Calzetti et al. (2000) to all the objects in the higher redshift bin with no Hγ flux, in order to ensure a direct comparison of our results with previous works.

6   METALLICITY

Given the large variety of different strong line metallicity calibrations used in the literature (see e.g. Pagel et al. 1979, Pettini & Pagel 2004; Kewley & Dopita 2002; Dopita et al. 2006; Tremonti et al. 2004; Nagao et al. 2006), which give very different results for a given line ratio, it is mandatory to study the evolution of the FMR using the same calibration used in M10. Consistently with that work, gas-phase metallicities were computed using the calibrations obtained by Nagao et al. (2006) and Maiolino et al. (2008), to allow a proper comparison with local SDSS galaxies. These ratios have been empirically calibrated at low metallicities $(12 + log(O/H) < 8.4)$ using direct T_e measurements in local metal poor galaxies and HII regions, and are based on the photoionization models by Kewley & Dopita 2002 (hereafter KD02) at high metallicity. The metallicity is therefore provided on the KD02 scale, while a conversion to other metallicity systems can be found in Kewley & Ellison (2008). The calibration proposed in KD02 is dependent on the [NII]/[OII] ratio, but the use of a secondary element as Nitrogen is of some concern. This issue will be addressed in detail by Maiolino et al. (in preparation, see also Pérez-Montero & Contini 2009a, Torres-Papaqui et al. 2011).

Two different measurements of metallicity are available for the two redshift ranges. At $z < 0.47$, where Hα is still visible, the [NII]/Hα ratio is used. At $z > 0.49$, where [OII] emission is in the accessible wavelength range, the measurement is instead based on the R_{23} quantity, defined as R_{23}=([OII]λ3727+[OIII]λ4959+[OIII]λ5007)/Hβ. In this latter case, as the lines involved are significantly separated in wavelength, the extinction correction discussed is Section 5 has to be applied to the observed line fluxes. Moreover,

as R_{23} has two possible metallicity solutions for a given line ratio, other diagnostics have to be used to remove the degeneracy and distinguish between the two branches at low and high metallicity.

We use for this task both the [OIII]/[OII] and [NeIII]/[OII] line ratios, which have a monotonic dependence on metallicity, but are also affected by a larger dispersion due to their additional dependence on the ionization parameter (see Nagao et al. 2006). In spite of their larger scatter, low and high metallicity galaxies are reasonably well separated in both diagrams (see e.g. Fig. 5 in Maiolino et al. 2008).

We therefore assigned all galaxies with log([OIII]/[OII])< 0.45 and log([NeIII]/[OII])< −0.6 to the high metallicity R_{23} branch, while all the others to the low metallicity one. The two independent branch indicators used agree for all the galaxies in our sample, supporting our method to discriminate between branches.

To further check the reliability of the branch selection done, we add to the galaxies used in Nagao et al. (2006) and Maiolino et al. (2008) the sample of ~ 600 SDSS with direct T_e measurement of Kniazev et al. (2004). We find that their galaxies with $S/N > 5$ on the [OIII]λ4363 line (used for T_e measurement, see e.g. Izotov et al. 2006) follow our criteria on [OIII]/[OII] to discriminate between the two branches. This is also confirmed by a larger sample of galaxies with T_e measurement that will be presented in a forthcoming paper (Maiolino et al. in preparation).

The uncertainties on the gas phase metallicities are of the order of $0.1 - 0.2$ dex, and are dominated by the spread in the calibrations themselves. The uncertainties in the higher redshift bin tend to be larger when the metallicity has values $12 + \log(O/H) \sim 8$, where R_{23} has a maximum and a small uncertainty in the line ratio produces a large uncertainty in metallicity. In any case, we note that just very few galaxies in our sample are in the low metallicity region where R_{23} is flat (between $12+\log(O/H) \sim 7.7 - 8.4$, see Fig. 4)

7   SAMPLE SELECTION

The results of the SED and emission line fitting described in Sect. 3 and 4 above were combined and used to define the two final subsamples (galaxies at $z < 0.47$ with accessible Hα emission and galaxies at $z > 0.49$ with [OII] emission). We applied to the initial sample discussed in Section 2 the following selections:

(i) each zCOSMOS spectrum is assigned to a confidence class according on the reliability of the final redshift. We selected all the objects with confidence classes 3 and 4 (respectively, "secure" and "very secure" redshifts), and class 2.5 (redshift with reliability larger than 85% and photometric redshift in good agreement with the spectroscopic redshift). We also added all the objects in classes 23 and 24, i.e. secondary targets detected in a slit positioned on another target, but with secure and very secure redshifts. We further excluded from our sample duplicate objects. Galaxies classified as broad-line AGN in the zCOSMOS catalog

(class > 10) or stars (class $*.4$) are automatically excluded from our selection.

(ii) as our two subsamples may be still contaminated by type-2 narrow line AGNs, or with by AGN with nuclear emission diluted in the host galaxy light, we applied two additional filterings. First, we excluded objects associated to X-rays selected AGN from the XMM-COSMOS catalog with rest-frame hard X-rays luminosity in excess than $2 \cdot 10^{42}$ erg s^{-1}, typical of AGNs (see Brusa et al. 2010 for more details). Second, to further exclude Compton Thick and Low Luminosity AGN below the XMM-COSMOS sensitivity, we used standard BPT selections based on emission line ratios. Following Bongiorno et al. (2010), we used the [OIII]/Hβ versus [NII]/Hα diagnostic diagram (Kauffmann et al. 2003b) for galaxies at $z < 0.46$, and the [OIII]/Hβ versus [OII]/Hβ diagram (Lamareille et al. 2004) for galaxies at $z > 0.49$;

(iii) the velocity shift between each fitted emission line centroid and the zCOSMOS redshift must be below 280 km/sec, and the line width must be between 110 km/sec and 290 km/sec, otherwise the fit is considered unreliable and the galaxy is excluded. For this selection we considered all the main emission lines: Hβ and [OIII]$\lambda5007$ for all the galaxies, Hα and [NII]$\lambda6548$ for galaxies at low redshift ($z<0.46$), [OII]$\lambda3727$ for galaxies at high redshift ($z>0.49$);

(iv) the same lines must not correspond to bright sky lines, or to spectral regions badly affected by fringing ($\lambda > 8000$ Å);

(v) the reduced χ^2 of SED fitting must be below 5, and the final 68% uncertainty on mass must be below 0.30 dex;

(vi) a threshold on the S/N of Hα and Hβ is also applied to have reliable and unbiased metallicity measurements. As line ratios depend strongly on metallicity (see, for example, Maiolino et al. 2008), applying the same thresholds to all relevant lines or to their ratios would introduce severe biases in metallicity (see M10 for a detailed discussion). To avoid these biases, and following what has been done for M10, we only apply high S/N thresholds to the lines which are diagnostics of SFR like Hα and Hβ. The actual threshold values depend on the redshift and stellar mass: at z<0.46 we used S/N(Hα)=15 for $log(M_*/M_\odot) \geqslant 9.4$, and S/N(H$\alpha$)=30 for $log(M_*/M_\odot) < 9.4$. At $z > 0.49$ we used S/N(Hβ)=8 for $log(M_*/M_\odot) \leqslant 9.8$, and S/N(H$\beta$)=20 for $log(M_*/M_\odot) > 9.8$. With these choices all the other relevant lines are detected with adequate S/N without additional, metal dependent selections. Indeed, in our lower redshift bin biases on metallicity are important mainly at low stellar masses: for example, at $log(M/M_\odot) \sim 9$, where metallicities are 12+log(O/H)$\sim$ 8.5, [NII] is only ~ 0.1 Hα, while at $log(M/M_\odot) \sim 10.2$, where the metallicity is as high as 12+log(O/H)$\sim$ 9, [NII] is ~ 0.4 Hα, and a lower S/N threshold on Hα may be applied to maximize the number of galaxies in our sample. In the higher redshift bin, on the other hand, the situation is reversed and [OIII], which is only ~ 0.4 Hβ in the high mass bin, increases to ~ 3 Hβ at the lower masses and metallicities.

These considerations indicate that our choice of S/N thresholds on Hα and Hβ lines that depends on mass in both redshift bins maximize the number of galaxies selected without introducing metallicity biases;

(vii) following M10, we checked the metallicity derived from [NII]$\lambda6548$/Hα for galaxies at $z < 0.46$ using an in-
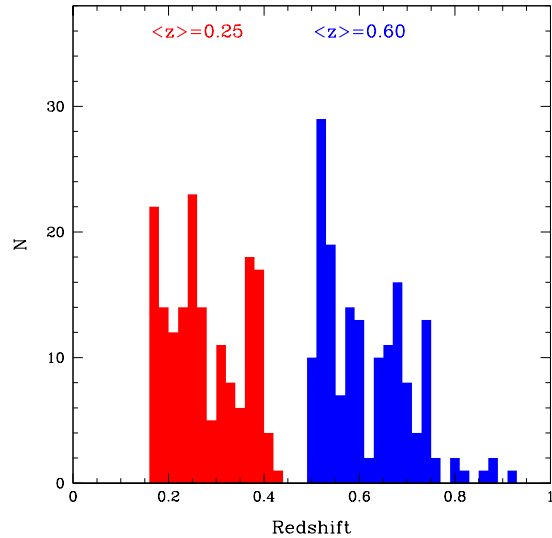
Figure 3. Redshift distribution of the two final galaxy subsamples (see text). The galaxies at $z < 0.47$ with visible Hα emission are shown in red, and galaxies at $z > 0.49$ with [OII] emission are shown in blue.

dependent metallicity indicator. As [OII] is not available in this redshift range, we used [OIII]/Hβ, which has properties similar to R_{23} with just a slightly larger scatter: we selected only galaxies where the values of metallicity obtained with the two different indicators differ less that 0.25 dex. At $z > 0.49$, instead, no additional independent metallicity tracer with low enough scatter is available, and no additional selection is applied;

After applying all these selections, we obtain 169 galaxies at $z < 0.47$ ($< z >= 0.25$) and 165 galaxies at $z > 0.49$ ($< z >= 0.60$). The redshift distribution of the two final subsample is shown in Fig. 3.

8 RESULTS

The Mass-Metallicity relations for the two zCOSMOS samples at $z \sim 0.25$ and $z \sim 0.60$ are shown in Fig. 4 (left panels). As expected, the Mass-Metallicity relation for the $z \sim 0.25$ sample is comparable to the relation derived by M10 for SDSS galaxies, as the SDSS sample used by M10 is including galaxies up to $z \lesssim 0.3$.

In the higher redshift bin, consistently with what was observed in other samples at comparable redshift (e.g. Savaglio et al. 2005, Cowie & Barger 2008, Rodrigues et al. 2008, Lamareille et al. 2009, Pérez-Motero et al. 2009b, Zahid et al. 2011), we find significant evolution of the mass metallicity relation, of ~ 0.1 dex. Moreover, if we plot the single galaxies on the mass metallicity relation color coded as a function of their SFR, as shown in Fig. 5 (left panels) for both redshift bins, there is a trend for more star forming galaxies to have lower metallicity at a given stellar mass, as found by M10 for the SDSS sample.

M10, in fact, defined the FMR adding the SFR of the
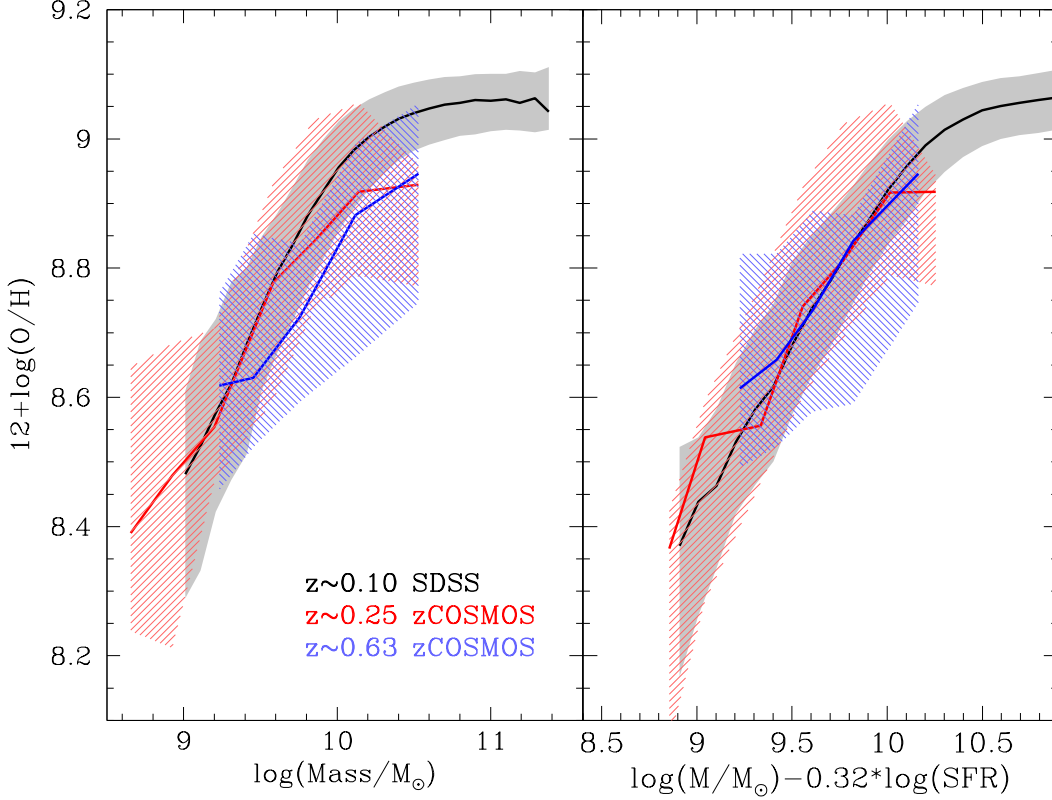
Figure 4. The mass metallicity relation (left panel) and the $\mu_{0.32}$ projection of the Fundamental Metallicity Relation (right panel) for the $z < 0.46$ (red solid lines) and the $z > 0.49$ (blue solid lines) zCOSMOS galaxies. The shaded areas contain galaxies between the 16th and the 84th percentile rank. The two high redshift relations are compared with the local one, as defined by the SDSS galaxies from M10 (black solid lines). It is evident an evolution of the mass metallicity relation at $z > 0.49$, while the corresponding projections on the FMR plane shows no evidence of evolution even at the higher redshift.

galaxies as a third parameter in the mass metallicity relation, showing that SDSS galaxies with lower metallicity also have higher SFR at a given mass, and that roughly half of the scatter in the relation was due to the different individual SFR of the galaxies. They also showed that the metallicity scatter of local galaxies could be minimized plotting them on a particular projection of the FMR, introducing a new quantity $\mu_{0.32}$ defined as:

$$\mu_{0.32} = log(M/M_\odot) - 0.32 \cdot log(SFR) \qquad (1)$$

As shown in the right panel of Fig. 4, no evolution is observed even in the higher redshift bin in the $\mu_{0.32}$ plane, once the increased SFR of the zCOSMOS galaxies at high z with respect to the local SDSS galaxies is accounted for. Moreover, the projection clearly removes any dependence of the mass-metallicity scatter from the SFR of the galaxies (see Fig. 5, right panels). This shows that the star forming galaxies up to $z \sim 0.8$ populate the same tight surface in the 3D space defined by their mass, metallicity and SFR as demonstrated by M10 for local SDSS galaxies.

To better check the presence of any evolution of the FMR with redshift, we compute the expected metallicity of each galaxy, given its stellar mass and SFR, according to the 3D plane defined by local SDSS in M10. We then plot in Fig. 6 the difference of the observed value with the expected

metallicity. The galaxies in both redshift bins are consistent with no differences from the FMR, with an average offset of $9 \cdot 10^{-3} \pm 0.17$ at $z < 0.46$ and $9 \cdot 10^{-3} \pm 0.16$ at $z > 0.49$, confirming with a much larger sample the no evolution of the FMR up to $z \sim 0.8$ suggested by M10.

The larger observed scatter in the zCOSMOS data with respect to the SDSS galaxies of M10 is partly due to instrumental effects. In fact, the VIMOS spectra used here are affected by significant fringing beyond ~ 8000 Å (see e.g. Le Fèvre et al. 2005). Although we excluded galaxies with emission lines in particularly bad part of the spectrum, our line fitting quality is anyway degraded redward of ~ 8000 Å. In fact, if we exclude the galaxies with emission lines contaminated by fringing (i.e. galaxies at $z > 0.22$ for our lower redshift bin and objects at $z > 0.6$ for the higher redshift bin), the scatter is significantly reduced to 0.11 dex and 0.14 dex respectively for the two subsamples. Moreover, the scatter in the local FMR based on SDSS galaxies depends significantly on mass and SFR, increasing at higher SFR and lower stellar mass (see Table 1 in M10). Therefore, the scatter derived for the zCOSMOS objects has to be compared with that obtained for SDSS galaxies with comparable stellar mass and SFR only: the $z = 0$ scatter corresponding to the lower redshift zCOSMOS subsample galaxy properties is 0.10 dex, while the one
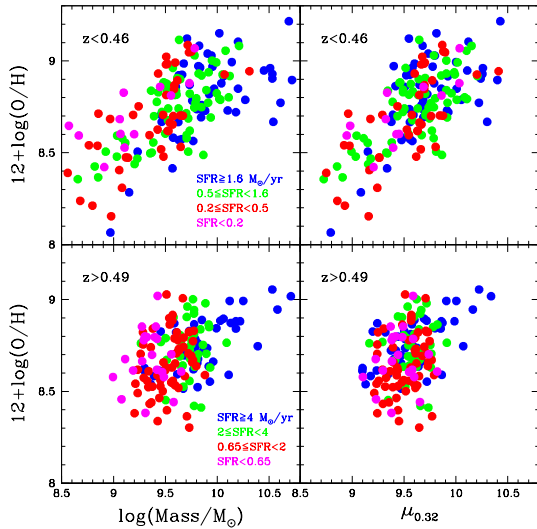
Figure 5. The mass metallicity relation (left panels) and the $\mu 0.32$ projection of the FMR (right panels) for the individual galaxies of the sample. The lower redshift bin ($z < 0.46$) is shown in the upper panels, while the higher redshift bin ($z > 0.49$) in the lower panels. The galaxies are color coded as a function of their SFR, with decreasing SFR from blue to magenta. While a trend for lower metallicity at higher SFR and fixed mass is present in the mass metallicity relation at both redshifts, the projection removes such effects, showing that the galaxies up to $z \sim 0.8$ populate a 3D plane defined by mass, metallicity and SFR as local SDSS galaxies.

Figure 6. Difference from the FMR surface for the zCOSMOS galaxies at $z < 0.46$ (left panel) and $z > 0.49$ (right panel) as a function of stellar mass. The single points are shown color coded as a function of their specific SFR, while their average in each bin along with the 1σ scatter is shown in black. The galaxies in both redshift bins are consistent with no differences from the FMR, with an average offset of $9 \cdot 10^{-3} \pm 0.17$ at $z < 0.46$ and $9 \cdot 10^{-3} \pm 0.16$ at $z > 0.49$. No residual dependencies from the SSFR is found.

relative to higher redshift one is 0.11 dex, closer to the fringing free scatter observed in our data. The remaining difference in the higher redshift bin is probably due to the single metallicity indicator used for those galaxies, while in M10 the abundances were derived using both R_{23} and Hα for all the galaxies.

The redshift evolution of the FMR based on the zCOS-MOS data presented in this work and on higher redshift data from the literature compiled by M10 is shown in Fig. 7. All the galaxy samples up to z=2.5 are consistent with no evolution of the FMR defined locally, while metallicities lower by ~ 0.6 dex are observed at $z = 3.3$ (see M10). As the data points at $z > 1$ are based on few massive galaxies, the larger samples at high redshift presented here at $z \sim 0.25$ and $z \sim 0.63$ provide a stronger evidence for the no-evolution of the FMR with redshift.

9   CONCLUSIONS

In this paper we have studied the gas phase metallicity of a sample of more than 300 star forming galaxies between $0.2 \lesssim z \lesssim 0.8$ from the zCOSMOS survey. We have measured the gas phase metallicity using strong optical line ratios, [NII]λ6548/Hα for galaxies at $z < 0.46$ and R_{23} for galaxies at $z > 0.49$.

We find that the metallicity of the galaxies is tightly related to their stellar mass, as for local galaxies. However,

a clear evolution of the mass metallicity relation of ~ 0.1 dex with respect to the local one is observed for the galaxies with $z > 0.49$. We also found a dependence of the scatter observed around the mass metallicity of our sample on the SFR, showing that star forming galaxies up to $z \sim 0.8$ are defining a 3D plane between stellar mass, metallicity and SFR, as local SDSS galaxies. Moreover, we have shown that projecting the galaxies on the FMR plane using the $\mu_{0.32}$ quantity successfully removes the dependence of the scatter by the SFR of the galaxies, and that on this projection the higher redshift zCOSMOS galaxies follow the relation defined by local SDSS galaxies with no evidences of evolution. The lack of evolution of the FMR at $0.2 < z < 0.8$ is fully confirmed for the zCOSMOS sample, as the expected metallicities computed according to the local FMR using the mass and SFR of the galaxies are consistent with the observed ones: the average offset is $9 \cdot 10^{-3} \pm 0.17$ at $z < 0.46$ and $9 \cdot 10^{-3} \pm 0.16$ at $z > 0.49$. The observed scatter is somehow larger than the one measured for SDSS galaxies, although the difference is probably due to VIMOS instrumental effects and to the lower number of independent metallicity indicators available.

The results presented confirm with much higher level of significance that the same physical processes are probably responsible for the SFR, metal enrichment and gas recycling through infall and outflows in the local and higher redshift Universe, as already suggested by M10. Moreover, they support the idea that the observed evolution of the mass-metallicity relation, at least up to $z \sim 0.8$, is simply due to more severe selection biases at high redshift as well as to
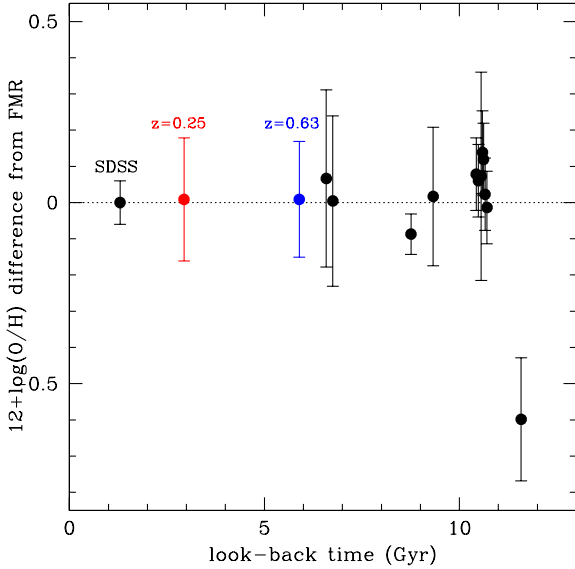
Figure 7. Redshift evolution from the FMR plane defined by local SDSS galaxies for zCOSMOS galaxies (this work, red and blue) and other high-z sample in the literature ($0.5 < z < 0.9$: Savaglio et al. 2005; $1.0 < z < 1.6$: Shapley et al. 2005, Liu et al. 2008, Wright et al. 2009, Epinat et al. 2009; $2.0 < z < 2.5$: Law et al. 2009, Förster Schreiber et al. 2009; $z \sim 3.3$: Maiolino et al. 2008, Mannucci et al. 2009). All the galaxy samples up to z=2.5 are consistent with no evolution of the FMR defined locally, while metallicities lower by ~ 0.6 dex are observed at $z = 3.3$. While each black point at $z > 0.7$ is the average of ~ 20 galaxies or less, the points at $z \sim 0.25$ and $z \sim 0.60$ comprise ~ 160 galaxies each.

the increase of the average SFR, which results in sampling different parts of the same FMR at different cosmic epochs.

Acknowledgments

REFERENCES

Bolzonella, M., Miralles, J.-M., & Pelló, R. 2000, A&A, 363, 476

Bolzonella, M., Kovac, K., Pozzetti, L., Zucca, E., Cucciati, O., et al., 2010, A&A, 524, 76
Bongiorno, A., et al. 2010, A&A, 510, A56
Brusa, M., et al. 2010, ApJ, 716, 348
Bruzual, G., & Charlot, S., 2003, MNRAS, 344, 1000
Capak, P., Aussel, H., Ajiki, M., McCracken, H. J., Mobasher, B., et al., 2007, ApJS, 172, 99
Calzetti, D., Armus, L., Bohlin, R. C., Kinney, A. L., Koornneef, J., et al., 2000, ApJ, 533, 682
Chabrier, G., 2003, ApJ, 586, 133
Cowie, L. L., & Barger, A. J. 2008, ApJ, 686, 72
Cresci, G., Mannucci, F., Maiolino, R., Marconi, A., Gnerucci, A., & Magrini, L. 2010, Nature, 467, 811
Davé, R., Finlator, K., & Oppenheimer, B. D. 2011, MNRAS, 1158
Dopita, M. A., et al. 2006, ApJS, 167, 177
Ellison, S. L., Patton, D. R., Simard, L., & McConnachie, A. W. 2008, ApJL, 672, L107
Epinat, B., Contini, T., Le Fèvre, O., et al. 2009, A&A, 504, 789
Erb, D. K., Shapley, A. E., Pettini, M., Steidel, C. C., Reddy, N. A., & Adelberger, K. L. 2006, ApJ, 644, 813
Erb, D. K. 2008, ApJ, 674, 151
Erb, D. K., Pettini, M., Shapley, A. E., Steidel, C. C., Law, D. R., & Reddy, N. A. 2010, ApJ, 719, 1168
Fontana, A., et al. 2004, A&A, 424, 23
Förster Schreiber, N. M., et al. 2009, ApJ, 706, 1364
Frayer, D. T., Sanders, D. B., Surace, J. A., Aussel, H., Salvato, M., et al., 2009, AJ, 138, 1261
Guillaume, M., Llebaria, A., Aymeric, D., Arnouts, S., & Milliard, B., 2006,
Ilbert, O., Capak, P., Salvato, M., Aussel, H., McCracken, H. J., et al. 2009, ApJ, 690, 1236
Izotov, Y. I., Stasińska, G., Meynet, G., Guseva, N. G., & Thuan, T. X. 2006, A&A, 448, 955
Kassin, S. A., et al. 2011, arXiv:1107.2931
Kauffmann, G. et al. 2003, MNRAS, 341, 33
Kauffmann, G., et al. 2003, MNRAS, 346, 1055
Kennicutt, R. C., Jr. 1998, ARAA, 36, 189
Kewley, L. J., & Dopita, M. A. 2002, ApJS, 142, 35
Kewley, L. J., & Ellison, S. L. 2008, ApJ, 681, 1183
Kniazev, A. Y., Pustilnik, S. A., Grebel, E. K., Lee, H., & Pramskij, A. G. 2004, ApJS, 153, 429
Lamareille, F., Mouhcine, M., Contini, T., Lewis, I., & Maddox, S. 2004, MNRAS, 350, 396
Lamareille, F., et al. 2009, A&A, 495, 53
Lara-López, M. A., et al. 2010, A&A, 521, L53
Law, D. R., Steidel, C. C., Erb, D. K., et al. 2009, ApJ, 697, 2057
Le Fèvre, O., Vettolani, G., Garilli, B., et al. 2005, A&A, 439, 845
Lilly, S. J., et al. 2007, ApJS, 172, 70
Lilly, S. J., et al. 2009, ApJS, 184, 218
Liu, X., Shapley, A. E., Coil, A. L., Brinchmann, J., & Ma, C.-P. 2008, ApJ, 678, 758
Maiolino, R., et al. 2008, A&A, 488, 463
Mannucci, F., et al. 2009, MNRAS, 398, 1915
Mannucci, F., Cresci, G., Maiolino, R., Marconi, A., & Gnerucci, A. 2010, MNRAS, 408, 2115
Mannucci, F., Salvaterra, R., & Campisi, M. A. 2011, MNRAS, 414, 1263
Maraston, C., 2005, MNRAS, 362, 799

Nakajima, K., et al. 2011, arXiv:1105.2824

Nagao, T., Maiolino, R., & Marconi, A. 2006, A&A, 459, 85

Pagel, B. E. J., Edmunds, M. G., Blackwell, D. E., Chun, M. S., & Smith, G. 1979, MNRAS, 189, 95

Pérez-Montero, E., & Contini, T. 2009, MNRAS, 398, 949

Pérez-Montero, E., et al. 2009, A&A, 495, 73

Pettini, M., & Pagel, B. E. J. 2004, MNRAS, 348, L59

Pozzetti, L., Bolzonella, M., Lamareille, F., Zamorani, G., Franzetti, P., et al., 2007, A&A, 474, 443

Pozzetti, L., Bolzonella, M., Zucca, E., Zamorani, G., Lilly, S., et al., 2010, A&A, 523, 13

Richard, J., Jones, T., Ellis, R., Stark, D. P., Livermore, R., & Swinbank, M. 2011, MNRAS, 413, 643

Rodrigues, M., et al. 2008, A&A, 492, 371

Savaglio, S., et al. 2005, ApJ, 635, 260

Shapley, A. E., Coil, A. L., Ma, C.-P., & Bundy, K. 2005, ApJ, 635, 1006

Steidel, C. C., Erb, D. K., Shapley, A. E., Pettini, M., Reddy, N., Bogosavljević, M., Rudie, G. C., & Rakic, O. 2010, ApJ, 717, 289

Surace, J. A., et al., 2004, VizieR Online Data Catalog, 2255, 0

Torres-Papaqui, J. P., Coziol, R., & Ortega-Minakata, R. A. 2011, arXiv:1107.5819

Torrey, P., et al. 2011, arXiv:1107.0001

Tremonti, C. A., et al. 2004, ApJ, 613, 898

Wright, S. A., Larkin, J. E., Law, D. R., et al. 2009, ApJ, 699, 421

Yates, R. M., Kauffmann, G., & Guo, Q. 2011, arXiv:1107.3145

Zahid, H. J., Kewley, L. J., & Bresolin, F. 2011, ApJ, 730, 137

Zamojski, M. A., Schiminovich, D., Rich, R. M., Mobasher, B., Koekemoer, A. M., et al., 2007, ApJS, 172, 468